Porous Polymer Films

DOI: 10.1002/anie.201407230

Directional Photomanipulation of Breath Figure Arrays**

Wei Wang, Can Du, Xiaofan Wang, Xiaohua He, Jiaping Lin, Lei Li,* and Shaoliang Lin**

Abstract: *Porous polymeric films are of paramount importance in many areas of modern science and technology. However, processing methods typically based on direct writing, imprint, and lithography techniques have low throughput and are often limited to specific fabricated shapes. Herein, we demonstrate the directional photomanipulation of breath figure arrays (BFAs) formed by an azobenzene-containing block copolymer to address the aforementioned problems. Under the irradiation of linearly polarized light, the round pores in the BFAs were converted to rectangular, rhombic, and parallelogram-shaped pores in 30 min, due to the anisotropic mass migration based on the photo-reconfiguration of the azobenzene units. Through a secondary irradiation after rotating the sample by 90°, the transformed pores were apparently recovered. Therefore, this non-contacted, directional photomanipulation technique in conjunction with breath figure processing opens a new route to nano/microporous films with finely tuned features.*

Polymeric films with highly ordered porous structures have attracted significant interest due to their potential application in the fields of separation, tissue engineering, photonic band gaps, micro-electronics, and lithography.[1] It is well known that the pore shape and size has significant influence on the practical applications of porous films. For example, the reaction of cells in a living tissue is controlled by the surrounding topography. The patterned surface can modulate cell adhesion and concomitant behavior, such as morphological changes and expression of cell function.[2] However, the often used methods are typically based on direct writing, imprint, and lithography techniques, have low throughput, and are limited in scope. Only specifically fabricated shapes can be created.[3] Breath figure (BF) is a facile and high-throughput method to prepare highly ordered polymer films, and has attracted increased attention in the past two decades.[4] When a polymer solution in a water-immiscible solvent is cast under high humidity, the rapid evaporation of solvent causes the temperature of the solution surface to drop, thereby initiating the nucleation of water droplets on the solution surface. These microdroplets are stabilized by the instant precipitation of a polymer layer around them, and self-assemble into a hexagonal array driven by the Marangoni convection. After total evaporation of the solvent and water, ordered pores are left on the polymer film surface, which are termed breath figure arrays (BFAs).[4]

Generally, the formed BFAs possess hexagonal close packing with microscale round pores. By controlling the direction and velocity of airflow during the evaporation, round pores in the BFAs can be transformed into ellipses.[5] In addition, a variety of physical secondary processing was also employed to create novel micro/nanostructured BFAs. Either mechanical stretching or shrinking can transform hexagonally arranged round pores, e.g., to square, rectangular, and triangular pores.[2a,6] Moreover, the pit size also decreases down to the nanoscale. To achieve this goal, the as-prepared porous film with BFAs has to be transferred from the solid substrate onto the surface of a shrinkable substrate.[6] Besides, the employed polymers should exhibit viscoelasticity in conformity with the distortion stress during the process to avoid film rapture. Therefore, a much simpler, noncontact technique is highly desired from both scientific and practical viewpoints.

The photomanipulation technique is a simple, green, and noncontact strategy.[7] Under the irradiation of linearly polarized light (LPL), azobenzene units selectively absorb light with the polarization direction parallel to their transition moments. Combining the polarization-selective *trans*-to-*cis* isomerization and unselective *cis*-to-*trans* back isomerization, the number of azobenzene moieties with their transition moments normal to the light polarization direction gradually increases, resulting in the light-selective alignment, with transition moments of azobenzenes almost perpendicular to the polarization direction of the actinic light. This is well known as the Weigert effect,[8] which distinguishes the azobenzene-containing polymers from other photosensitive or photochromic materials. The mass migration based on the photoreconfiguration of azobenzene units in the azobenzene-containing polymers is called photofluidization, which not only allows nanoscopic elements of materials to be precisely manipulated with good repeatability and high throughput,[9] but also causes massive motion in microscale and tunes the

[*] W. Wang,[+] X. Wang, Prof. J. Lin, Prof. S. Lin
Shanghai Key Laboratory of Advanced Polymeric Materials
Key Laboratory for Ultrafine Materials of Ministry of Education
School of Materials Science and Engineering
East China University of Science and Technology
Shanghai 200237 (China)
E-mail: slin@ecust.edu.cn
C. Du,[+] L. Li
College of Materials, Xiamen University
Xiamen 361005 (China)
E-mail: lilei@xmu.edu.cn
Prof. X. He
Department of Chemistry, East China Normal University
Shanghai 200241 (China)
E-mail: xhhe@chem.ecnu.edu.cn
[+] These authors contributed equally to this work.

[**] This work was supported by the National Natural Science Foundation of China (51103044, 21174038, 51373143, 51035002, and 21174116), the Projects of Shanghai Municipality (11A1401600, 13ZZ041, and 12JC1403102), and the Fundamental Research Funds for the Central Universities (NCET-12-0857, WD1213002, 2013SH003, and 201312G004).

Supporting information for this article is available on the WWW under http://dx.doi.org/10.1002/anie.201407230.

polymer aggregation.[10] Herein, we report the directional photomanipulation of BFAs formed by an azo-containing diblock copolymer. Depending on the polarization direction of the incident light and the irradiation time, the original round pores of BFAs are converted into rectangular and rhombic structures. After rotating the sample by 90°, anisotropic photofluidization causes the transformed pores to recover, except for the shrinkage along the *z* direction vertical to the film surface.

The preparation of the azobenzene-containing block copolymer, poly(4-vinylpyridine)-*block*-poly[6-[4-(4-butylphenylazo)phenoxy]hexyl methacrylate] (P4VP-*b*-PAzoMA), and the static BF processing are described in detail in the Supporting Information (SI). The chemical structure of P4VP-*b*-PAzoMA is shown in Figure 1a. After

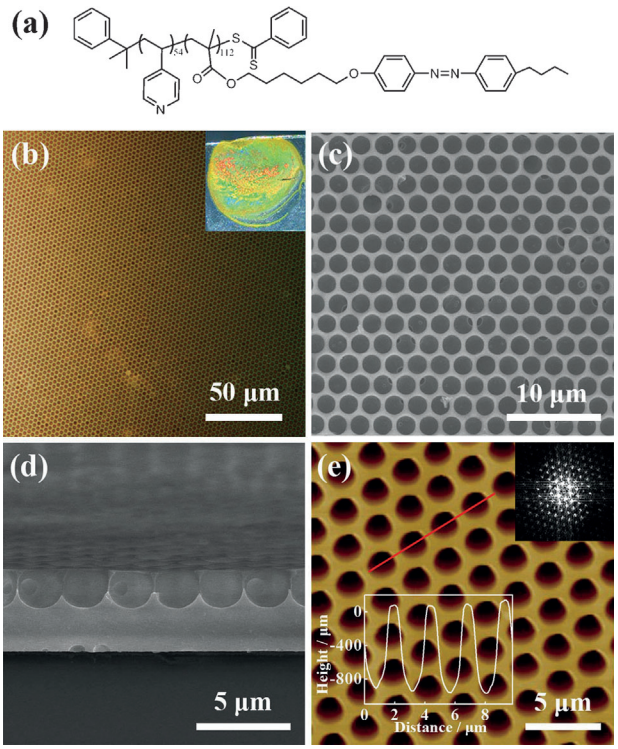

Figure 1. a) The chemical structure of the P4VP-*b*-PAzoMA copolymer. b) Optical microscopy image of the honeycomb film formed from P4VP-*b*-PAzoMA copolymers, inset: photograph of sunlight diffraction of the film. SEM images of the honeycomb structured film; c) top view; d) cross-section view. e) Topographic image of the honeycomb structured film, insets: fast Fourier transform (FFT) of the image.

BF processing, the obtained film exhibits nacre color due to sunlight diffraction and interference effects (see the inset of Figure 1b) on the highly ordered surface features. An optical microscopy (OM) image (Figure 1b) shows that the area of defect-free BFAs is in the square millimeter range. More precise microscopy investigation by scanning electronic microscopy (SEM) demonstrates that the film is composed of a monolayer of hexagonally arranged pores on a dense base layer (Figure 1c and d). The pore size is 2.0 μm with a pore-to-pore distance of 2.5 μm, which is corroborated by atomic force microscope (AFM) measurements. The corresponding fast Fourier transform (FFT) of the AFM image (inset in Figure 1e), with the appearance of first- and high-order spots indicates that the main structure is of high regularity.

To investigate the dependence of the pore transformation on the light polarization and irradiation time, the obtained porous films were exposed under a vertical incident LPL with a wavelength of 450 nm and a density of 1400 mW cm^{-2}, as schematically shown in Figure 2a. Different from thermally

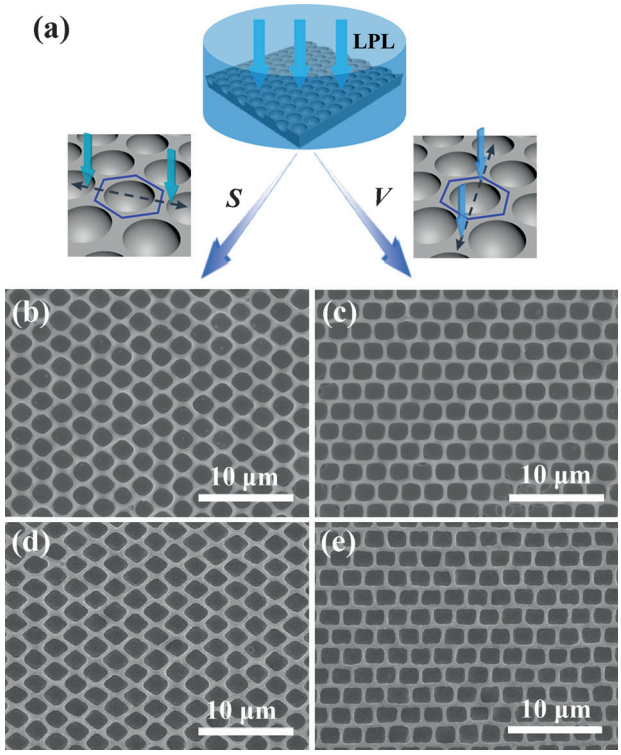

Figure 2. Schematic and SEM images of the photo-reconfiguration patterns for different light polarization and irradiation times. a) Two types of irradiation; deformed BFAs after irradiation along the *S* direction and the *V* direction for 10 min (b,c) and 30 min (d,e), respectively.

induced isotropic reflow, the photo-induced reconfiguration provides unprecedented flexibility to control the structural features, because the polarization direction of the incident light is the only factor determining the direction of anisotropic fluidity.[9a,11] Therefore, two characteristic polarization directions of LPL are chosen in the hexagonal lattice model. As illustrated in Figure 2a, one is the *S* direction (from the center of the pore to the side of the honeycomb hexagon) and the other is the *V* direction (from the center of the pore to the vertex of the honeycomb hexagon). Depending on the irradiation time and the polarization direction, a spectrum of transformative microstructures is developed eventually. When the light polarization was along the *S* direction, round pores were converted into round-rhombic pores after 10 min irradiation, as shown in Figure 2b. Further irradiation for additional 20 min generated rhombic pores (Figure 2d). For the *V* direction irradiation, the round pores were deformed to

a round-rectangle shape (Figure 2c) in 10 min. After 30 min irradiation, a rectangular shape could be observed, as shown in Figure 2e. The deformation behavior and surface morphological variance were also confirmed by AFM (SI, Figure S3). Both the calculated and the measured transmission confirm that the light intensity within a piece of the azobenzene polymer film gradually decreases and eventually becomes almost zero at a thickness of 800 nm.[12] Additional SEM cross-sectional views (SI, Figure S4) also demonstrate the slight shrinkage of the contour of the BFA pores in the *z* direction, indicative of the mass migration near the surface skin. Therefore, the actual action of photofluidization is the expansion and elongation of the BFAs in the direction parallel to the light polarization in the *xy* plane due to the photo-induced reconfiguration, accompanied by a contraction against the polarization direction due to the isovolumetric effect.[13]

Based on the hexagonally packed pores, a unit cell is drawn as the rhombic area of $O_1O_2O_3O_4$ (*O* indicates the center of the pore), to illustrate the deformation mechanism as schematically shown in Figure 3a. The shadow part is magnified and represents the deformation unit (DU), where the middle points of pores are denoted by capital letter, *C*. The points A and B are the barycenter of the triangle-connected pores. For the honeycomb structure, the value of l_2 (the length between A and B) is twice that of l_1 (the length between the middle point and the adjacent barycenter). In the case of the *S* direction irradiation as shown in Figure 3b, the propagation of the incident LPL is perpendicular to the direction of AB. Due to the directional photofluidization, the sides of DU tend to shrink along the AB direction. Such a mass transport causes A and B to approach each other, leading to the decrease of l_2 and the increase of l_1, and the transformation of round pores into rhombic structures with increasing irradiation time. Conversely, when the light polarization is along the *V* direction, the sides of DU tend to elongate along the AB direction, which increases l_2 and decreases l_1, resulting in a conversion of the round pores to the rectangular shape. In fact, the surface features can be finely tuned by simply changing the polarization direction of the incident light for the unprecedented directionality of photofluidization. For example, BFAs with parallelogram-shaped pores were prepared after 30 min irradiation along the direction between the *S* and *V* direction (SI, Figure S5).

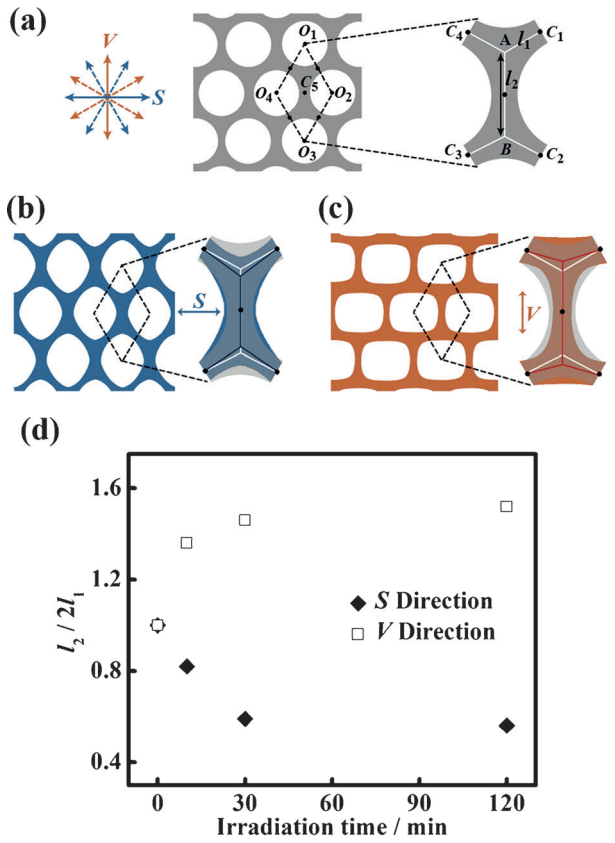

Figure 3. The lattice and deformation unit model of pristine (a) and deformed BFAs for the irradiation along the *S* direction (b) and *V* direction (c). d) Plots of $l_2/2l_1$ versus the irradiation time for the two types of irradiation direction.

The real variation of the value of $l_2/2l_1$ versus the irradiation time was measured and plotted in Figure 3d. The values achieve a maximum of 1.46 in the *V* direction, whereas a minimum of 0.59 is obtained in the *S* direction after 30 min irradiation. Further increasing the irradiation time to 2.0 h (SI, Figure S6), did not change these values significantly, suggesting that the re-alignment of the azobenzene groups in the surface layer has been completed in 30 min.

It should be noted that the photofluidization depends on the intensity of the LPL. The irradiation of BFAs under a weaker light (280 mW cm^{-2}) was carried out for comparison (SI, Figure S7). The results clearly showed that the photofluidization of the azobenzene groups became slower under weak light, leading to a lower degree of photoinduced deformation of BFAs.

The transformed BFAs also demonstrate the apparent restorability by subsequent irradiation after rotating the sample by 90° with an equal time intervals. Starting from the rhombic pores induced by irradiation along the *S* direction for 30 min, the BFAs with round pores were almost recovered after subsequent irradiation along the *V* direction for another 30 min, as shown in Figure 4a. The value of $l_2/2l_1$ is 0.94, which is close to that in the originally as-prepared film. The SEM cross-sectional view in Figure 4b shows that the contour of the pores changes from a round to an ellipse, indicating that the shrinkage of BFAs in the *z* direction can tolerate the massive motion during the irradiation.

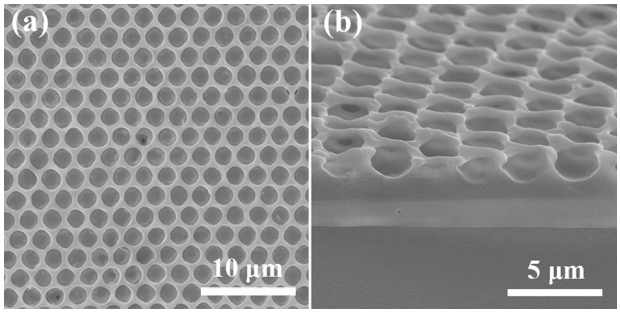

Figure 4. SEM images of micropatterns after a secondary photomanipulation. a) Top view; b) cross-sectional view.

In summary, we developed a facile, high-throughput, and noncontact photomanipulation strategy for the preparation of porous polymeric films with finely adjustable pore shape. Round pores in the BFAs can be converted into rectangular, rhombic, and parallelogram-shaped structures in 30 min, depending on the polarization direction of the incident light with respect to the orientation of the arrays. Furthermore, the transformed pores in the BFAs apparently can be restored with a secondary irradiation after rotating the sample by 90°. As such, the directional photofluidization technique in conjunction with BF processing offers very promising engineering applications, avoiding the need for the direct writing, imprint, and expensive lithographic techniques. We believe that such a photomanipulation strategy, in conjunction with molecular design, can be implemented in other azobenzene-containing polymers, to produce various types of porous films with further functionalization.

Experimental Section

P4VP-*b*-PAzoMA diblock copolymer was synthesized by a two-step RAFT polymerization. First, the macromolecular RAFT agent P4VP-SC(S)Ph was synthesized by a typical RAFT polymerization of 4-vinylpyridine (4VP) using cumyl dithiobenzoate (CDB) as a RAFT agent in dimethylformamide (DMF). Then, the target diblock copolymer P4VP-*b*-PAzoMA was synthesized by a second RAFT polymerization of 6-[4-(4-butylphenylazo)phenoxy]hexyl methacrylate (AzoMA) using P4VP-SC(S)Ph as a macromolecular RAFT agent in DMF. For the preparation of BFAs, a static breath-figure process was operated in a glass vessel with a constant relative humidity of 83.6%. The copolymer was dissolved in CH_2Cl_2 with a concentration of 1.0 wt%. The micropatterned film was prepared by casting the polymer solution with a microsyringe onto a glass substrate placed in the vessel. For photoinduced reconfiguration of the honeycomb structure, the samples were irradiated by a vertical incident LPL with a wavelength of 450 nm. Detailed experimental information is given in the SI.

Received: July 15, 2014
Revised: August 14, 2014
Published online: September 22, 2014

Keywords: block copolymers · breath figures · microarrays · photomanipulation · thin films

[1] A. Muñoz-Bonilla, M. Fernández-García, J. Rodríguez-Hernández, *Prog. Polym. Sci.* **2014**, *39*, 510 – 554.
[2] a) T. Nishikawa, M. Nonomura, K. Arai, J. Hayashi, T. Sawadaishi, Y. Nishiura, M. Hara, M. Shimomura, *Langmuir* **2003**, *19*, 6193 – 6201; b) D. Beattie, K. H. Wong, C. Williams, L. A. Poole-Warren, T. P. Davis, C. Barner-Kowollik, M. H. Stenzel, *Biomacromolecules* **2006**, *7*, 1072 – 1082.
[3] a) M. Deubel, G. Von Freymann, M. Wegener, S. Pereira, K. Busch, C. M. Soukoulis, *Nat. Mater.* **2004**, *3*, 444 – 447; b) M. S. Rill, C. Plet, M. Thiel, I. Staude, G. Von Freymann, S. Linden, M. Wegener, *Nat. Mater.* **2008**, *7*, 543 – 546; c) J. H. Zhang, Y. F. Li, X. M. Zhang, B. Yang, *Adv. Mater.* **2010**, *22*, 4249 – 4269; d) Y. Lei, S. K. Yang, M. H. Wu, G. Wilde, *Chem. Soc. Rev.* **2011**, *40*, 1247 – 1258.
[4] a) H. Bai, C. Du, A. Zhang, L. Li, *Angew. Chem. Int. Ed.* **2013**, *52*, 12240 – 12255; *Angew. Chem.* **2013**, *125*, 12462 – 12478; b) G. Widawski, M. Rawiso, B. Francois, *Nature* **1994**, *369*, 387 – 389.
[5] J. Li, J. Peng, W. Huang, Y. Wu, J. Fu, Y. Cong, L. Xue, Y. Han, *Langmuir* **2005**, *21*, 2017 – 2021.
[6] H. Yabu, R. Jia, Y. Matsuo, K. Ijiro, S. Yamamoto, F. Nishino, T. Takaki, M. Kuwahara, M. Shimomura, *Adv. Mater.* **2008**, *20*, 4200 – 4204.
[7] Y. Yu, M. Nakano, T. Ikeda, *Nature* **2003**, *425*, 145.
[8] a) F. Weight, *Verh. Dtsch. Phys. Ges.* **1919**, *21*, 479 – 483; b) K. G. Yager, C. J. Barrett, *J. Photochem. Photobiol. A* **2006**, *182*, 250 – 261; c) H. Yu, T. Kobayashi, *Molecules* **2010**, *15*, 570 – 603; d) A. Natansohn, P. Rochon, *Chem. Rev.* **2002**, *102*, 4139 – 4176; e) H. Yu, *Prog. Polym. Sci.* **2014**, *39*, 781 – 815.
[9] a) S. Lee, J. Shin, Y. H. Lee, S. Fan, J. K. Park, *Nano Lett.* **2010**, *10*, 296 – 304; b) H. Yu, T. Ikeda, *Adv. Mater.* **2011**, *23*, 2149 – 2180.
[10] a) Y. Li, Y. He, X. Tong, X. Wang, *J. Am. Chem. Soc.* **2005**, *127*, 2402 – 2403; b) Y. Wang, S. Lin, M. Zang, Y. Xing, X. He, J. Lin, T. Chen, *Soft Matter* **2012**, *8*, 3131 – 3138; c) S. Lin, Y. Wang, C. Cai, Y. Xing, J. Lin, T. Chen, X. He, *Nanotechnology* **2013**, *24*, 085602.
[11] a) S. Lee, H. S. Kang, J. K. Park, *Adv. Mater.* **2012**, *24*, 2069 – 2103; b) S. Lee, H. S. Kang, J. K. Park, *Adv. Funct. Mater.* **2011**, *21*, 1770 – 1778.
[12] H. S. Kang, S. Lee, S. A. Lee, J. K. Park, *Adv. Mater.* **2013**, *25*, 5490 – 5497.
[13] a) P. Karageorgiev, D. Neher, B. Schulz, B. Stiller, U. Pietsch, M. Giersig, L. Brehmer, *Nat. Mater.* **2005**, *4*, 699 – 703; b) Y. Gritsai, L. M. Goldenberg, J. Stumpe, *Opt. Express* **2011**, *19*, 18687 – 18695.

